X-ray sources in and behind strong-lensing clusters of galaxies

Vladi Pankrushin

Advisor: Dr. Adi Zitrin

Department Of Physics, Ben Gurion University

2023

Contents

1 Background and Motivation

X-ray sources can be found all across the sky. We would like to analyse the X-ray source density in clusters in comparison to their visible spectrum counterpart and compare to sources of both types outside clusters. In addition, we would like to search for gravitationally lensed X-ray sources in Chandra images, which are much harder to find than in Hubble images, in which an abundance of lensed optical features are seen. This direction of the project was incited by the recent discovery of a lensed X-ray source by M.B. Bayliss and M. McDonald [1], and by several known lensed quasars.

1.1 Source density

Clusters are defined as an overdensity of galaxies, but also baryonic matter more specifically as well as dark matter, so obviously the density of X-ray and visible spectrum sources is higher in them than outside. Around clusters we expect some statistical distribution of sources, while, possibly, having a peak or a jump around the virial shock radius. This is expected as in the virial shock's radius there is a jump in the gas density, which potentially may cause a higher source density. The reason we are interested in X-ray source overdensity is because in addition to the higher overall mass density, centers of galaxy clusters may exhibit more black holes and AGNs, which are known to be the primary sources of X-ray radiation in the universe. X-ray overdensities have been studied by other groups previously, for example [2].

1.2 Gravitational Lensing

Gravitational Lensing is a phenomenon affecting astronomical images by having a sufficient mass distribution between the source and the telescope. The effect is a product of the general theory of relativity, which predicts the deflection of light caused by the change in the space's geometry caused by the existence of massive objects. There are 3 classes of gravitational lensing:
Strong lensing - Strong distortions, creating Einstein rings, arcs and multiple images. Typical galaxy clusters will create a separation of a few tens of arcseconds between images.
Weak Lensing - Weak distortions, creating small shears that are hard to notice by eye and require a statistical analysis.
Microlensing - No noticeable distortion in shape, only a fluctuation of the light received from the background.
Note that in this project we will deal with strong lensing, which is of our main interest, although the sources we find may be also weakly magnified.
The deflection angle of gravitational lensing can be written as:

$$\vec{\hat{\alpha}} = -\int \vec{\nabla}_{\perp} n dl = \frac{2}{c^2}\int \vec{\nabla}_{\perp}\Phi dl$$

For $\vec{\hat{\alpha}}$ the diflection angle, Φ gravitational potential, dl the light's path and n the effective reflective index. The gravitational potential in Newtonian gravity is given by:

$$\Phi(b,z) = -\frac{GM}{(b^2+z^2)^{1/2}}$$

For b the impact parameter and z the position along the axis of the original movement direction. As shown in the following figure:

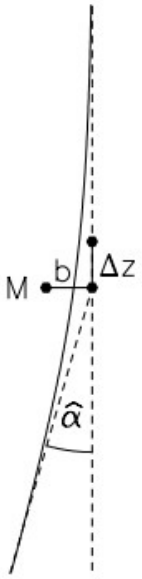

Figure 1: Light deflection by a point mass. Taken from [3]

By calculating the gradient we will get:

$$\hat{\alpha} = \frac{2}{c^2} \int \vec{\nabla}_{\perp} \Phi dz = \frac{4GM}{c^2 b}$$

For M the point mass and G the gravitational constant.
Following the thin screen approximation, we can project any 3-dimensional mass to a 2-dimensional mass density:

$$\Sigma(\vec{\xi}) = \int \rho(\vec{\xi}, z) dz$$

For Σ the 2-dimensional density, ρ the 3-dimensional density and $\vec{\xi}$ a 2-dimensional vector in the lens plane.
Making the deflection angle:

$$\vec{\hat{\alpha}}(\vec{\xi}) = \frac{4G}{c^2} \int \frac{(\vec{\xi} - \vec{\xi'})\Sigma(\vec{\xi'})}{\left|\vec{\xi} - \vec{\xi'}\right|^2} d^2\xi'$$

As shown in the following figure:

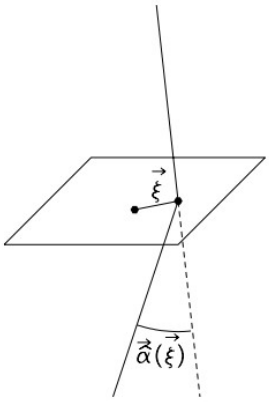

Figure 2: Thin screen approximation. Taken from [3]

In a typical gravitational lens system, where S is the source and I is the image, we will define new distances and angles as follows:

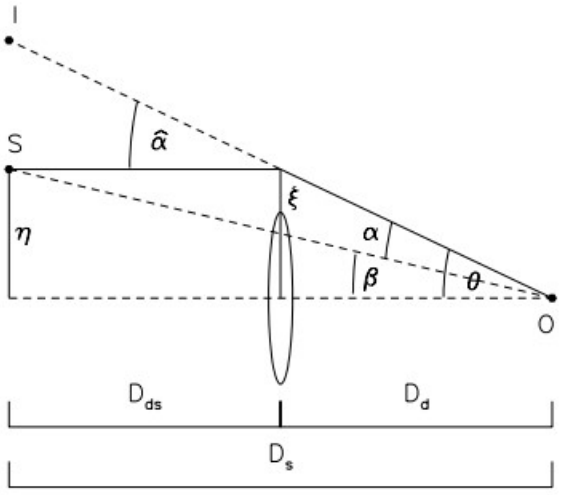

Figure 3: Gravitational lens system. Taken from [3]

This helps define the reduced deflection angle:

$$\vec{\alpha} = \frac{D_{ds}}{D_s}\vec{\hat{\alpha}}$$

Where the parameters are defined as in the figure above. Another important relation is the lens equation:

$$\vec{\beta} = \vec{\theta} - \vec{\alpha}(\vec{\theta})$$

With that, we can ask when $\beta = 0$ for all θ. Such densities are called critical densities. For a constant surface-mass density for example one might calculate the following critical density:

$$\Sigma_{cr} = \frac{c^2}{4\pi G}\frac{D_s}{D_d D_{ds}}$$

Densities higher than the critical one are called supercritical and usually those are the lens which produce several images to the same source. If the lens has a circular symmetry and a source is on the optical axis, a supercritical density will produce a ring as an image, those are called Einstein Rings.

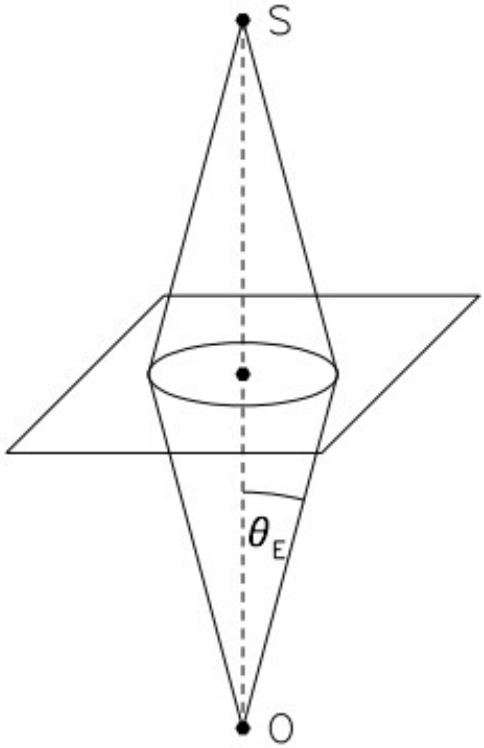

Figure 4: Einstein Ring and radius. Taken from [3]

The radius of such ring, called the Einstein radius would be:

$$\theta_E = [\frac{4GM(\theta_E)}{c^2}\frac{D_{ds}}{D_d D_s}]^{1/2}$$

If the source isn't perfectly aligned or there are fluctuations in the mass density in the lens, one will see images in the form of arcs instead of the ring. Images might also appear sheared in the direction perpendicular to the lens. Under various different configurations, one might see a combination of all the effects mentioned above (an arc, a sheared image and a deflected image). The deflection of light also changes the apparent solid angle of the source, while the surface brightness preserves, as described by Liouville's theorem. The total flux received is proportional to the ratio between the solid angles of the image and the source, defining magnification:

$$\text{magnification} = \frac{\text{image area}}{\text{source area}} := \mu$$

The magnification factor can be geometrically found by:

$$\mu = \frac{\theta}{\beta}\frac{d\theta}{d\beta}$$

1.3 Telescopes Used

We mainly used data provided by two telescopes: Hubble and Chandra. When Chandra provided the X-ray images and Hubble provided the visible spectrum images. Sites providing the data are listed in

the next subsection.

1.3.1 Chandra

A telescope measuring EM waves in the X-ray spectrum, wave lengths of $(0.12 - 12)nm$. A telescope with a diameter of $1.2m$, a focal length of $10m$, collecting area of $0.04m^2$ and resolution of $0.5arcsec$. Its' orbital path has a semi-major axis of $80,795.9km$, eccentricity of 0.743972 and a period of $3809.3min$.

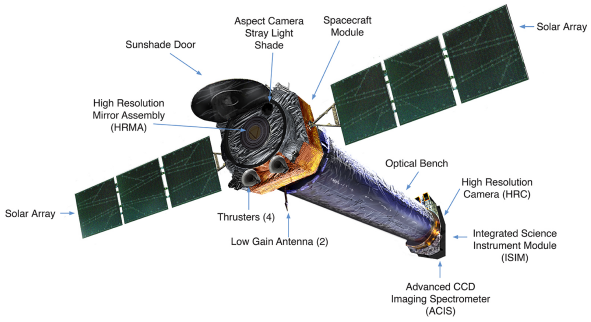

Figure 5: Chandra telescope. Taken from NASA

1.3.2 Hubble

A telescope measuring EM waves in the visible spectrum, near-infrared and ultraviolet, wave lengths of $(0.1 - 2.5)micron$. A telescope with a diameter of $2.4m$, a focal length of $57.6m$, collecting area of $4m^2$ and resolution of $0.014arcsec$. Its' orbital path has a semi-major axis of $6909km$, eccentricity of 0.00024 and a period of $95.42min$.

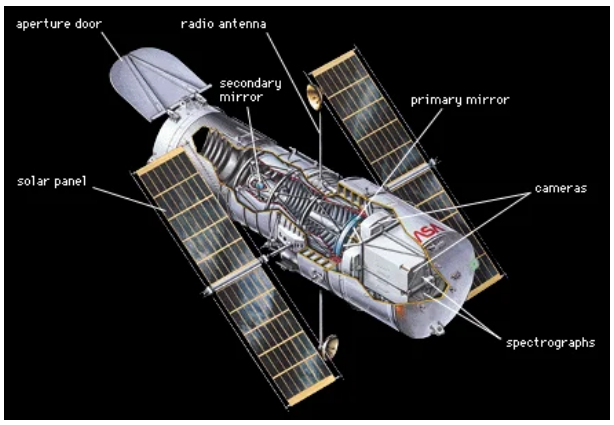

Figure 6: Hubble telescope. Taken from Britannica

1.4 Tools Used

The data used in the project was taken from the Chandra X-ray Center [4], Reionization Lensing Cluster Survey [5] and coordinates and redshifts were taken from RELICS Clusters [6]. Visualisation and various physical properties were measured by the SAOImageDS9 application. Further data analysis which was not covered by DS9 functions was made in Python (Google Colab).

1.5 RELICS

Reionization Lensing Cluster Survey (RELICS) is the group of clusters we will be using in this project. The clusters in this group are some of the heaviest clusters known, by measurements of the trace of gasses around clusters. Heavy clusters will fit our project well as those shall provide the most noticeable deflections in gravitational lensing and a large number of sources to calculate densities from.

2 Density Measurements

We would like to examine the amount and density of X-ray sources around clusters and figure out if those have a higher overdensity compared to the overdensity of sources of the visible spectrum seen in Hubble images.

2.1 Chandra

2.1.1 Method

We went through the RELICS list of clusters [5] and downloaded the data of all clusters that appeared also in our list of coordinates [6] and that were found in Chandra's database [4]. Those clusters amount to: A697, A1300, A2163, ACT-CLJ0102, CLJ0152.7, MACSJ0417.5, MACSJ0308.9, PLCKG004.5, PLCK171.9, PLCK287, PLCK138.61, RXCJ0142.9, RXCJ2211.7, RXCJ0018, RXCJ01514 and SPT-CLJ0615. We opened those images on DS9, used a Gaussian filter (of which the parameters were: Radius 3 and Sigma 1.5) and counted by eye the amount of sources we found. In addition, we measured physical properties like brightness, average brightness surrounding the source, size, distance from the center of the cluster and coordinates. Centers of cluster were picked as the brightest pixel in the area that was chosen by eye as being the center of said cluster. We plotted a histogram of the sources as a function of their distance from the center of their cluster. We divided each bin in the histogram by the circular area the bin encapsulates around the center of the cluster, to calculate the 2D density in each bin. In parallel, we searched for Chandra images outside of clusters: Extragalactic diffuse emission and surveys, solar systems, SN, SNR and isolated NS. From which we calculated the overall density in average.

2.1.2 Results

After counting all visible sources and measuring their distances from the cluster center, we analytically calculated the physical distances (in kpc) using the given angular distances and redshifts (assuming $H_0 = 67.04$, $\Omega_m = 0.3183$ and $\Omega_\Lambda = 0.6817$). We got the following histogram (dividing by 20 bins running between the closest and furthest source detected):

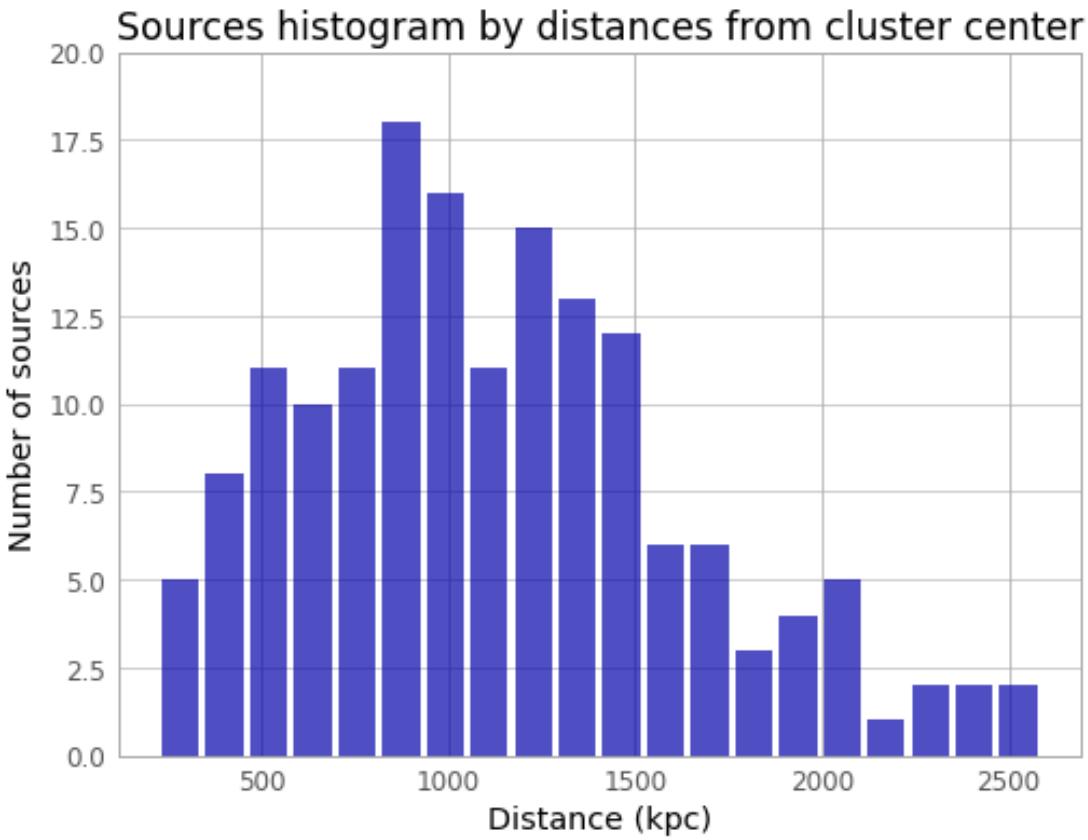

Figure 7: Histogram of sources by distance from cluster center, X-ray

We also plotted the distribution by redshift, to visualize the spread of redshifts in our data:

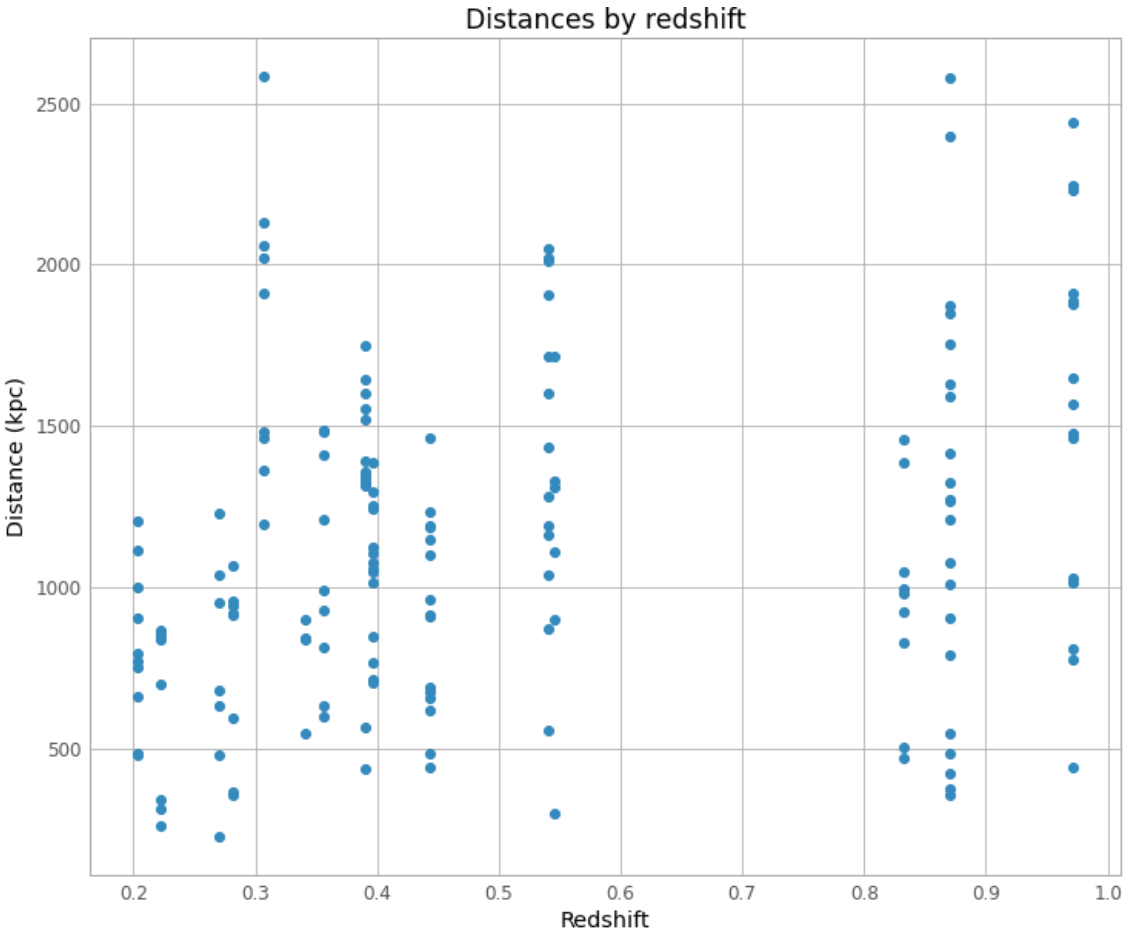

Figure 8: Sources distribution by redshift, X-ray

Dividing the data from figure 7 by the area, we plot the density graph:

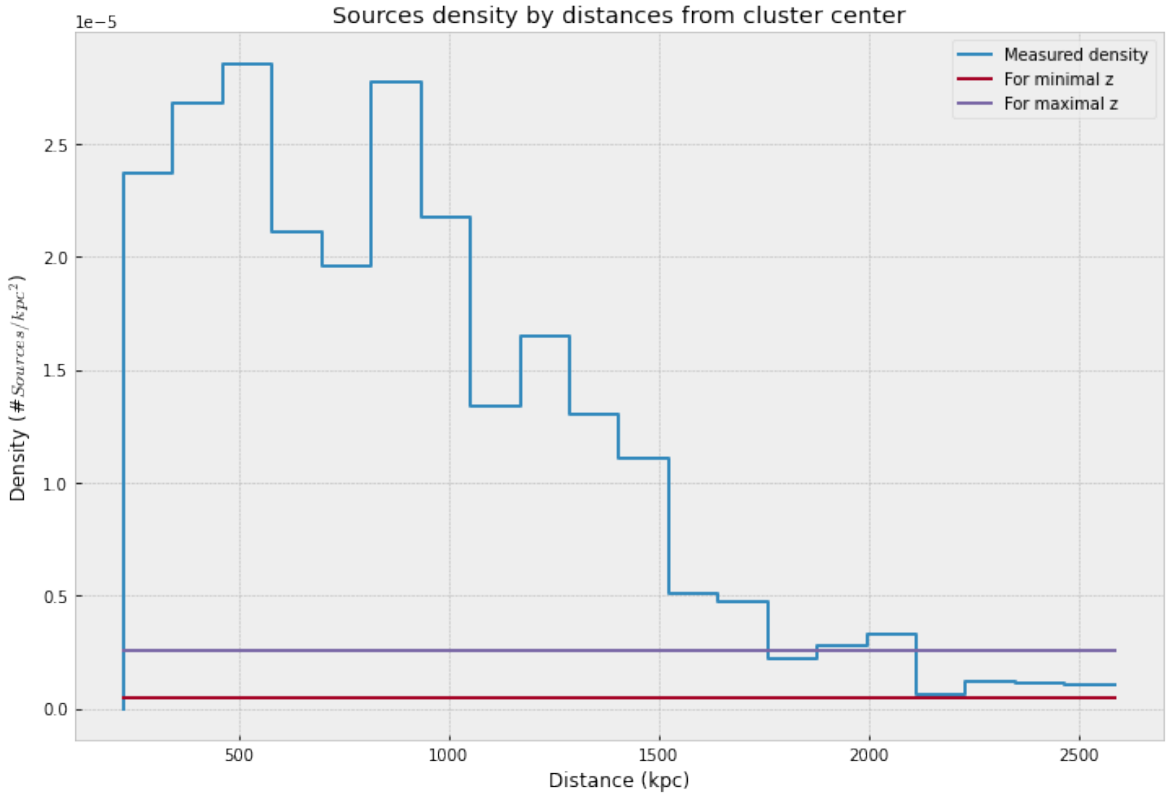

Figure 9: Density distribution by distance from cluster center, X-Ray

From the solar systems we gathered 8 images which averaged in 2.625 sources. From fields around SNs we gathered 2 images averaging 2.5 sources (excluding the SN itself as a source). From the extragalactic surveys we gathered 9 images averaging 8 sources.

Table 1: Extragalactic sources, Chandra

Name	**# of Sources**
1WGA1226.9	10
1WGAJ1340.1	2
A2534	3
A2554	11
Deep Field South CDF-S	13
Deep Field South CDF-N	11
Hubble Deep Field	7
Lockman Hole	2
NGC4244	13
Average	8

Averaging all of those together we get 5.15 sources per image.

The length of Chandra's images was measured to be $(8.407 \pm 0.002) arcmin$ which lead to an area of $(70.56 \pm 0.02) arcmin^2$. The average number of sources inside clusters divided by the area was $10.86/70.56 = (0.1534 \pm 0.02) arcmin^{-2}$. The density we measured through the graph (by the 'tail' of the gaussian fit) was $1.068 \cdot 10^{-6} kpc^{-2}$, meaning the comparison between the two measurements

Table 2: SNs, SNRs and NSs, Chandra

Picture	**Number of sources**
1	4
583	1
average	2.5

Table 3: Solar systems, Chandra

Picture	**Number of sources**
113	0
114	0
116	2
117	6
118	1
727	9
1387	1
1828	2
Average	2.625

depends on the redshift of said clusters. Our clusters were bounded by $z_{min} = 0.203, z_{max} = 0.972$, which translates into the densities:
$density_{min} = 0.0486 \cdot 10^{-5} arcmin^{-2}, density_{max} = 0.2583 \cdot 10^{-5} arcmin^{-2}$. Which we will notice fits the background density calculated prior.

(*) Notice that for cluster RXC0142, there were two centers detected, so we used the middle point between them.

To compare the overdensity to Hubble's result, let us plot the results in terms of angular distance:

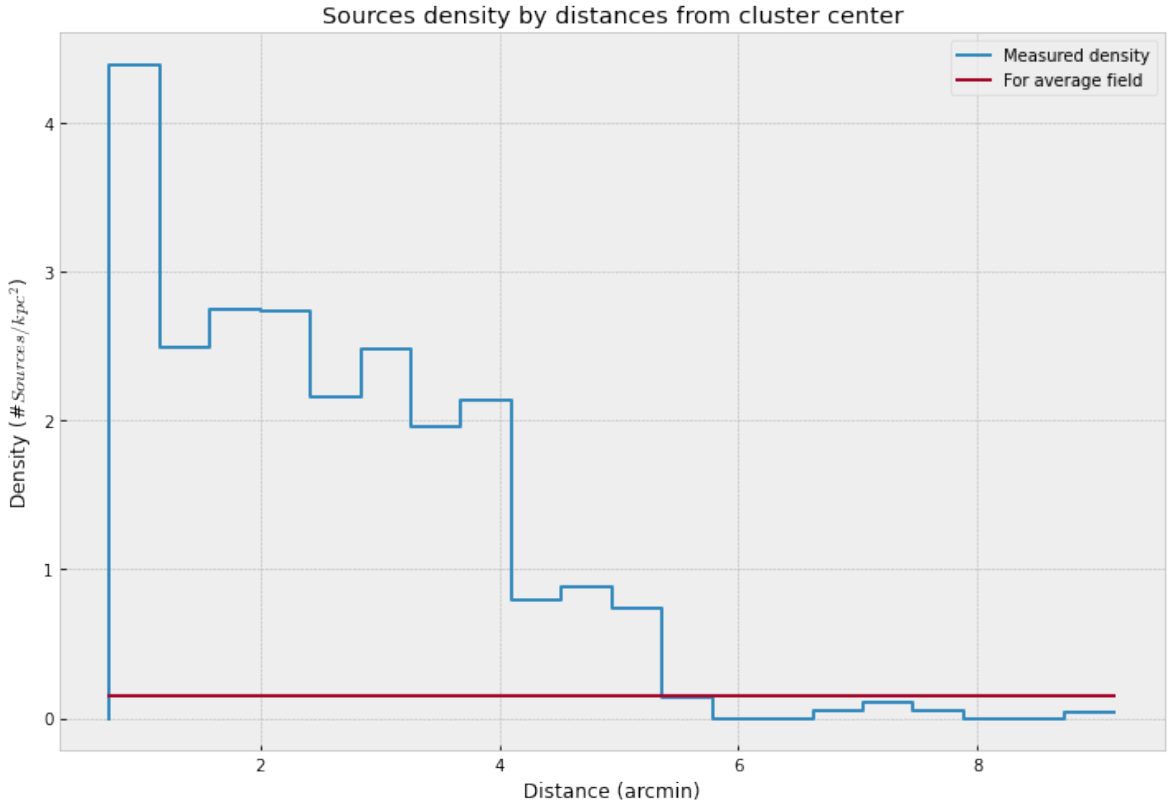

Figure 10: Density distribution by angular distance from cluster center, X-ray

We wish to also measure the overdensity specifically in the radii we managed to measure in the Hubble chapter. For that we've broken up the bins between $(0.7-1.0)arcmin$, which are the values the Hubble measurement cover, into 8 bins. We calculated in those 8 bins the ratio between the cluster density and the parallel field density, and averaged over them, leading to the result: 19.7 ± 9.

2.1.3 Conclusions

We managed to find and measure sources from the listed clusters and their distances. We also managed to find data from extragalactic images outside of clusters.

We see more sources in higher redshifts on average in figure 8 because we look at a broader area (same angular size, just further), therefore we expect seeing more sources on average.

The parallel field density was measured to be: $(0.1534 \pm 0.02)arcmin^{-2}$ or $(0.0486-0.2583) \cdot 10^{-5}kpc^{-2}$ depending on the redshift. The local ratio between the cluster density and the parallel fields' density in the $(0.7-1.0)arcmin$ was measured to be 19.7 ± 9.

In figure 9, we notice a local peak and a sudden drop at around $900kpc$ from the cluster centers. As previous research (see [7] and [8]) suggests virial shocks in galaxy clusters happen around $(0.5-2)Mpc$, we suspect a virial shock of the clusters' gas may potentially be the cause for those sudden drops in our measurements. Although it is a mere suggestion that requires further research and evidence.

2.2 Hubble

2.2.1 Method

We went through the following clusters: RXC0142, A697, PLCKG00419, PLCKG1310, PLCKG171, RXC2211 and RXC1514. We located the centers of the clusters by opening the images in DS9 and locating the brightest pixel in the brightest area that was chosen by eye. Then we downloaded the catalogs of each cluster, counted the number of provided sources and calculated their distances from their respective cluster centers. We plotted the histograms (by distance from the center) of each cluster, and then divided by area to plot the densities as a function of distance from the cluster distance. In addition, we took the catalog data for the parallel fields of each cluster and calculated the sources densities in each.

2.2.2 Results

For the parallel fields we calculated the following results:

Table 4: Parallel fields densities

Parallel field to	**Number of sources**	**Density** $(\#/arcmin^2)$
A1300	3590	143.6
A697	3187	127.5
PLCKG00419	6346	253.8
PLCKG13810	4481	179.2
PLCKG17140	3571	142.8
RXC0142	4117	164.7
RXC1514	3335	133.4
RXC2211	3666	146.6
Average	4036.625	161.45

As we see, we've got an average density of $(161 \pm 40) arcmin^{-2}$. The results we've got from the clusters, after averaging over the densities were:

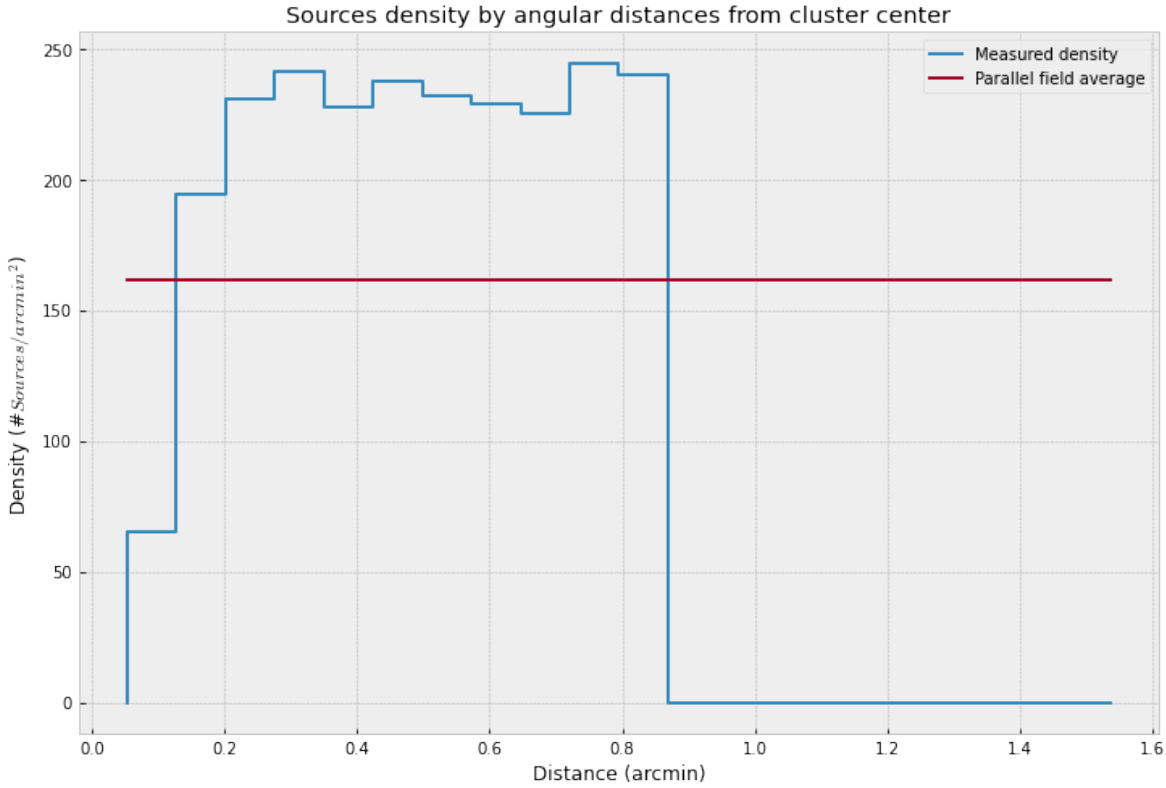

Figure 11: Average density by radius, Hubble

Notice we've cut the data for radii which surpassed the borders of the image, which means different bins (the few last ones shown in figure 11) were also averaged over different numbers of clusters. We took the values from the 4th bin to the 12th and averaged the ratio between the cluster density to the parallel fields density over them. The result we've got was 1.4 ± 0.1.

2.2.3 Conclusions

We counted the sources and plotted by radius from the cluster center, finding the overdensity to be 1.4 ± 0.1 times over the average in the parallel fields, which was measured to be 161 ± 40.

The density measured in X-ray was much higher in the measured boundaries compared to that of Hubble's spectrum. 19.7 ± 9 times the average of the control group, compared to 1.4 ± 0.1 we have here. So we definitely notice an overdensity of about 13.5 ± 6 times higher in the X-ray spectrum.

We are able to only judge by the ratio, and not the count, as the Hubble images are of a far higher resolution and are able to detect more sources, about 2 orders of magnitude higher than that of Chandra's.

There is a high uncertainty in our measurements, mainly because of the combination of two facts: The angular range of Hubble's images are much smaller than that of Chandra's, leaving only a small portion of our X-ray measurements being relevant as a comparison to Hubble's counterpart.
The resolution of Chandra's images being relatively very poor. Leading us to count only the brightest sources, which amount to about a few dozens per cluster (or a few hundreds over the entire data set). So by cutting our data to the radii relevant to Hubble's images, we are left with about 0 to 1 sources per cluster to base our overdensity on, which amounts to 7 sources over our entire data set. Which is of course a very low amount to base any statistics on. From figure 10 we might notice that the overall X-ray data suggests a lower overdensity than the one we calculated, as the Hubble-relevant radii are

around the peak of our density histogram. But as there are no Hubble data for those radii, it is difficult to draw any relative conclusions from the majority of the X-ray histogram. An important nuance to mention is the fact that sources which appear in our images aren't necessarily in the cluster, but could also be simply in the line of sight. We suppose the phenomenon doesn't differ greatly between X-ray and Hubble's spectrum, therefore it is unlikely to have a significant effect on our measurements.

3 Search for lensed sources

We tried finding gravitationally lensed X-ray sources following the method mentioned in M.B. Bayliss' team [1], by finding the easily recognizable lensed images in Hubble images (usually arcs) and searching for sources in Chandra's images in the exact coordinates.

3.1 Method

We went through all the clusters for which we have both Chandra and Hubble data for. For each cluster, we opened its' Hubble image in DS9 and searched by eye for lensed images and arcs. For each such source, we opened the corresponding Chandra image and by the 'lock WCS' function and looked for similar fluctuations in the same coordinates. Once we find such corresponding fluctuations, we would calculate the noise in the area using a gaussian fit, then calculate statistically how probable were the fluctuations there.

3.2 Results

We searched the following clusters (in both Chandra and Hubble): A697, A1300, A2163, ACT-CLJ0102, CLJ0152.7, MACSJ0417.5, MACSJ0308.9, PLCKG004.5, PLCK171.9, PLCK287, PLCK138.61, RXCJ0142.9, RXCJ2211.7, RXCJ0018, RXCJ01514, SPT-CLJ0615. Only one suspected source was found out of all of those clusters. In cluster MACS0417 we found the following 3 arcs:

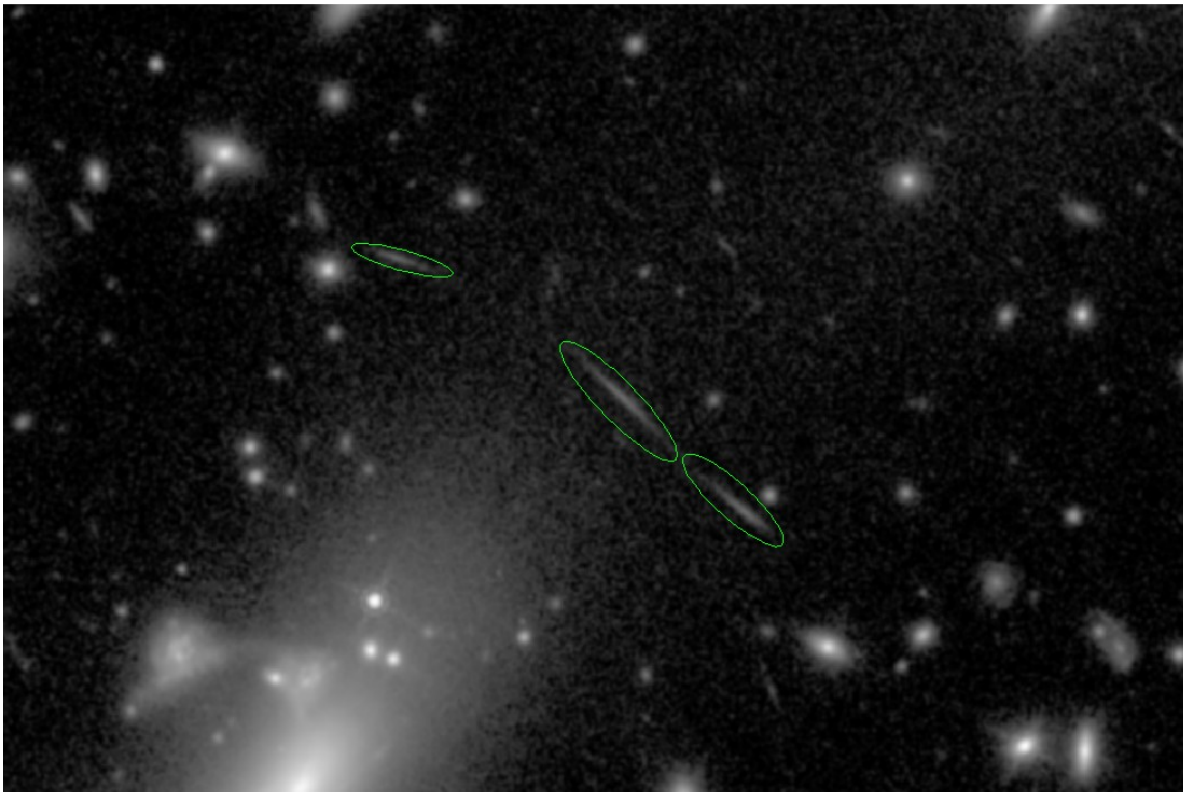

Figure 12: Hubble image of cluster MACS0417, the lensed sources being marked

The corresponding area of those arcs in Chandra's image is:

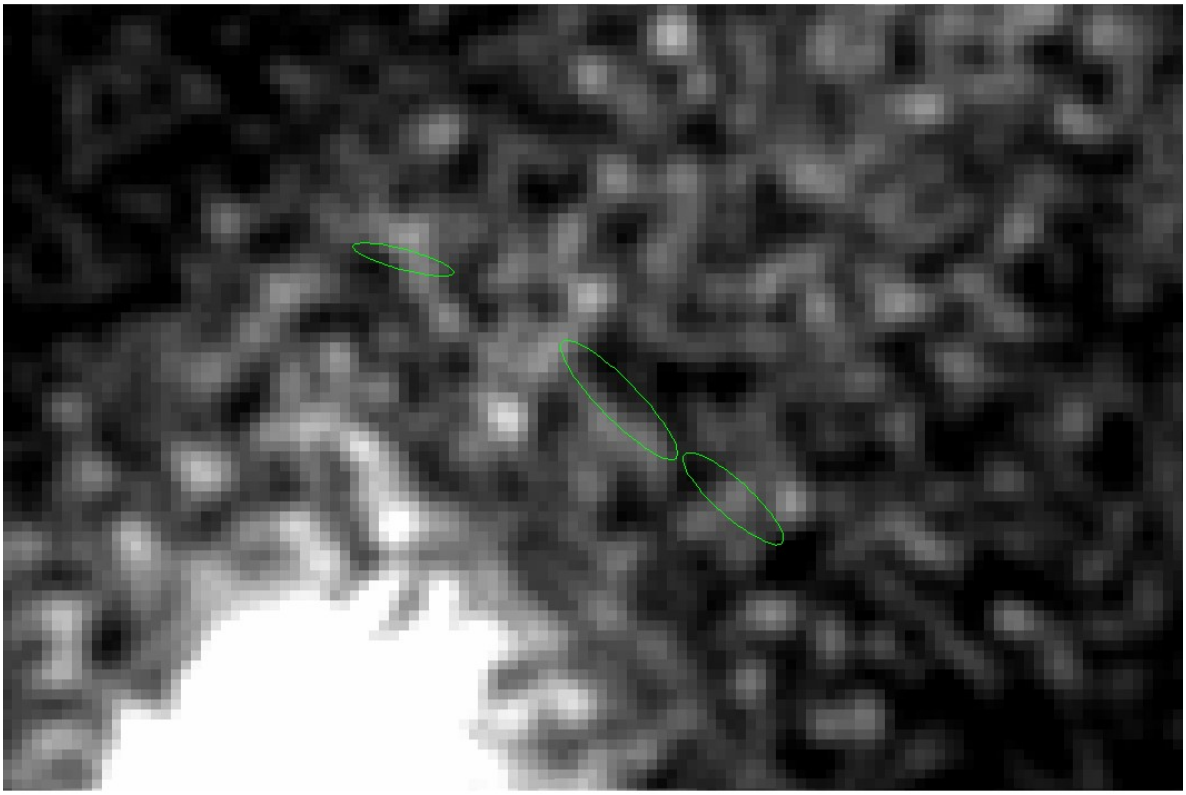

Figure 13: Chandra image of cluster MACS0417, the suspected lensed sources being marked

To calculate the fluctuations in the area we plotted the histogram for the following marked area:

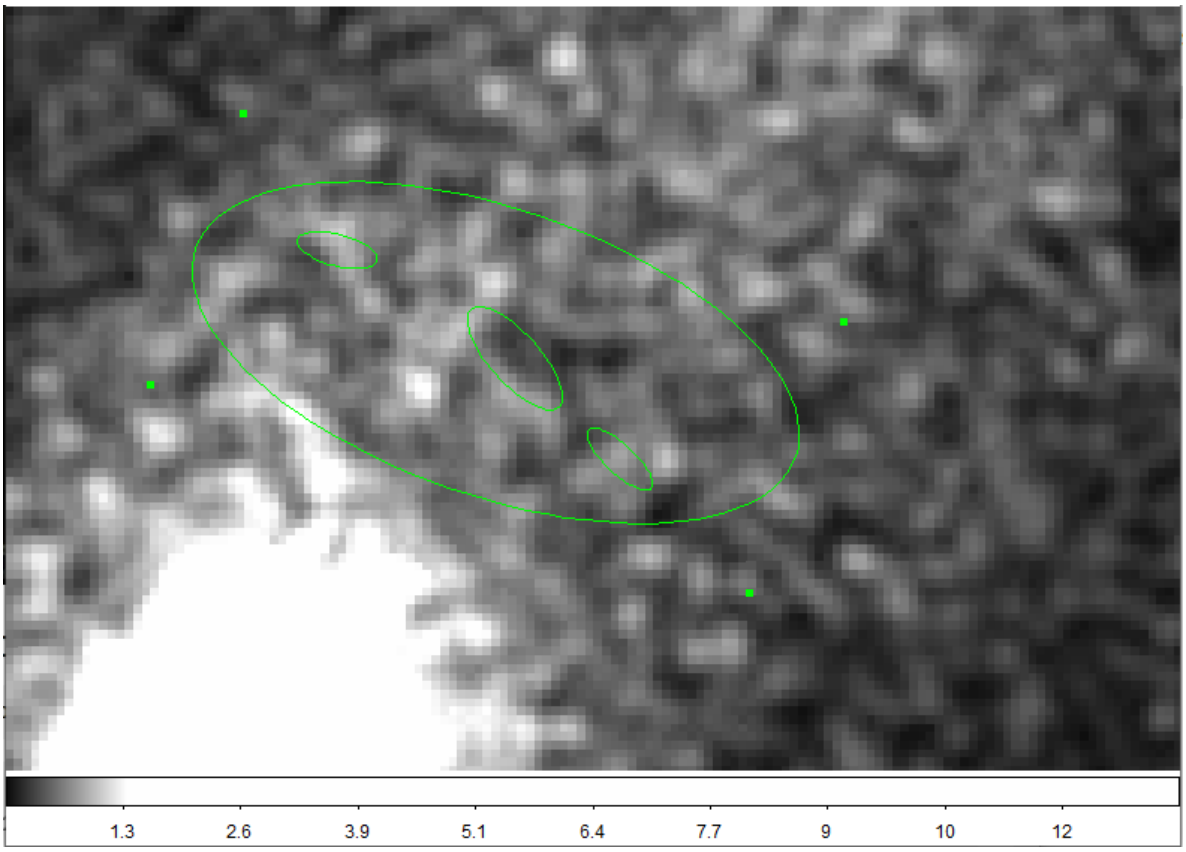

Figure 14: Chandra image of cluster MACS0417, area taken for fluctuations

The histogram of the pixels in the marked area were fit into a typical gaussian function: $y = a \cdot exp[-(x - x_0)^2/(2\sigma^2)]$, which led to the following results:

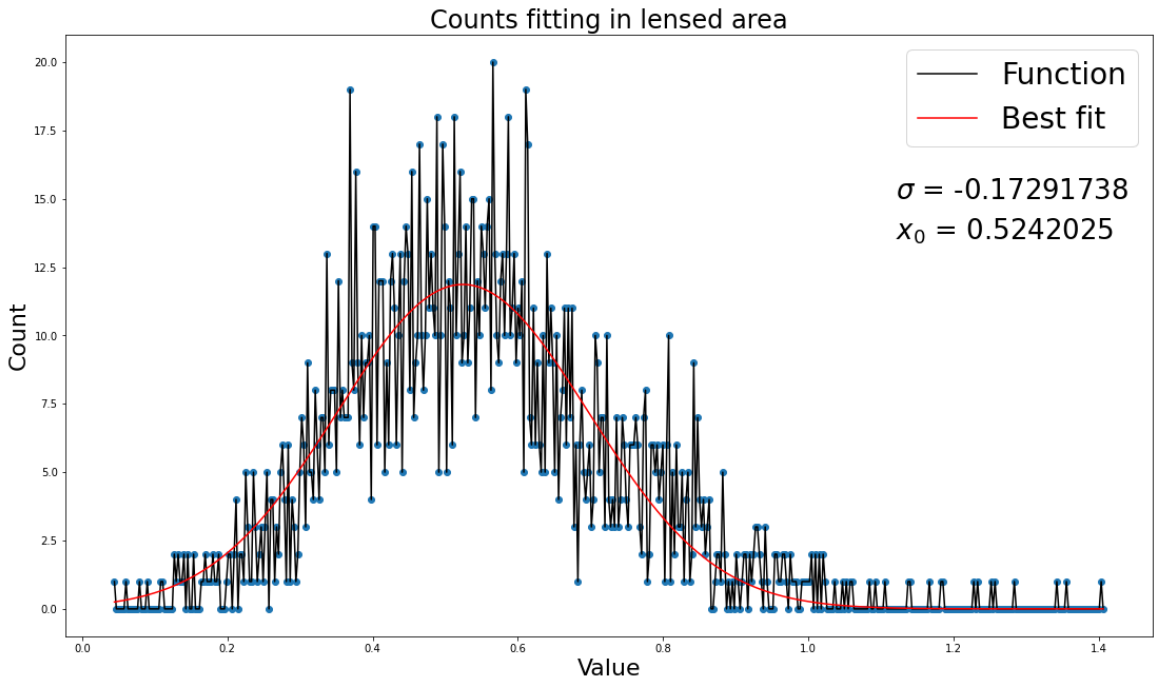

Figure 15: Gaussian fit to local histogram

The mean values of the pixels (in Chandra's image) where the arcs are, are: 0.688761, 0.497289, 0.592203. This leads to the likelyhood of those brighter areas being just fluctuations (in units of σ): 0.9510, 0.1556, 0.3932.

3.3 Conclusions

Finding matching sources was difficult, as most X-ray sources didn't appear in the visible spectrum and vice versa. Additionally, the poor resolution of the X-ray images made it difficult for them to be mapped to their visible spectrum counterpart. Most lensed sources and even entire arcs found in Hubble's images were significantly smaller than a single pixel in Chandra's image. The one suspected area is very likely to be simple fluctuations, as none of the 3 areas corresponding to the arcs in Hubble's image were even above 1σ.

References

[1] K. Sharon M.B. Bayliss, M. McDonald. An x-ray detection of star formation in a highly magnified giant arc, nature astronomy. 2019. doi: https://doi.org/10.1038/s41550-019-0888-7.

[2] Murat Hudaverdi Turgay Caglar. Xmm–newton view of x-ray overdensities from nearby galaxy clusters: the environmental dependencies. 2017. doi: https://doi.org/10.1093/mnras/stx1811.

[3] Matthias Bartelmann Ramesh Narayan. Lectures on gravitational lensing. 1995. doi: https://doi.org/10.1140/epja/s10050-020-00317-3.

[4] Smithsonian Astrophysical Observatory. Chandra x-ray: Chandra data archive. URL https://cda.harvard.edu/chaser/mainEntry.do.

[5] Dan Coe. Reionization lensing cluster survey (relics). URL https://cda.harvard.edu/chaser/mainEntry.do.

[6] Association of Universities for Research in Astronomy. Relics clusters. URL https://relics.stsci.edu/clusters.html.

[7] I.Khabibullin E.Churazov. Tempestuous life beyond r500: X-ray view on the coma cluster with srg/erosita. 2020. doi: https://doi.org/10.1051/0004-6361/202040197.

[8] Gregg Hallinan Uri Keshet, Kuan-Chou Hou. Synchrotron emission from virial shocks around stacked ovro-lwa galaxy clusters. 2022. doi: https://doi.org/10.48550/arXiv.2210.09317.